Journal of the Korean Physical Society (2023) 82:1171–1179
https://doi.org/10.1007/s40042-023-00789-8

Online ISSN 1976-8524
Print ISSN 0374-4884

ORIGINAL PAPER - CONDENSED MATTER

Structural and electronic properties of neutral boron clusters doped with two potassium atoms

Guo Li Chen[1] · Yu Quan Yuan[1] · Chun Ping Wang[2] · Ying Ying Wang[1] · Ting Liu[1] · Teng Xin Huang[1] · Wei Lin[3] · Jing Yang[1]

Received: 12 December 2022 / Revised: 30 January 2023 / Accepted: 16 February 2023 / Published online: 29 March 2023

Abstract
This paper reports a systematic study on the doping of two potassium atoms in small-sized neutral boron clusters. The CALYPSO software in conjunction with DFT was used to anticipate the low-energy structures, optimize their geometry, and adjust their energies. With increasing size, the structural development of the K_2B_n ($n = 1$–12) clusters was revealed, and we discovered that the majority of their ground-state structural isomers structurally inherited well from the corresponding ground-state isomers of pure B clusters. A fresh finding was made after confirming the NPA (natural population analysis) of the low-lying K_2B_n ($n = 1$–12): every doped K atom in the structure has a positive charge. According to relative stability analysis, the most stable K_2B_8 cluster within the parameters of our investigation has a HOMO–LUMO gap of 3.31 eV. Strong interactions between K-4s and B-2P AO were also discovered through an additional examination of the molecular orbitals and bonds of K_2B_8 clusters. These interactions may be the primary cause of K_2B_8's exceptional stability. We hope that our research will be useful in the future for synthesizing and using doped boron-based nanomaterials.

Keywords Cluster · CALYPSO · DFT · K_2B_n

1 Introduction

In recent years, boron-containing materials have attracted great interest and widespread attention from researchers due to their unique properties and promising applications. Due to their unparalleled properties, such as flame retardancy, heat resistance, high hardness, high strength, wear resistance, etc., and novel physicochemical properties, boron-containing materials have been used in industrial and agricultural production and serve people's life [1–3].

Boron atoms have small radii and high ionization potential. Atomic structure characteristics with electron deficiency determine the complexity of boron bonding. It is almost impossible for boron atoms to lose electrons to form ionic or metallic bonds, and due to its electron deficiency, it is difficult for boron to achieve all valence bonds as two-electron covalent bonds [4–7]. The boron atoms adopt the SP^3 hybridization state, accepting electron pairs with empty SP^3 orbitals, and reducing their electron deficiency through the formation of coordination bonds. Boron only possesses three valence electrons in its four valence orbitals, but it can still build stable coordination compounds by accepting lone electron pairs from multi-electron groups in its spare orbitals [8]. The boron atom adopts the SP^2 hybridization state to reduce its electron deficiency by forming delocalized π-bonds with empty 2P orbitals. This type of bonding exists in all molecules or atomic groups of the planar triangular configuration of boron [9–13].

Many studies on boron clusters have been conducted in recent years. Boron tends to form multicenter delocalized bonds to compensate for its electron-deficient nature, which determines the diversity of boron cluster structures. Theories and experiments support the notion that, at small sizes, boron clusters typically form stable planar (quasi-plane) structures [14, 15]. Through photoelectron spectroscopy (PES) and theoretical research, Wang's group discovered in

✉ Yu Quan Yuan
yuquan_yuan@suse.edu.cn

[1] School of Physics and Electronic Engineering, Sichuan University of Science and Engineering, Zigong 643000, China

[2] Department of Physics, Yichang SCG Display Devices Co., Yichang 443000, China

[3] Department of Physics, Chengdu Experimental Foreign Languages School, Chengdu 611134, China

2003 that the smaller boron clusters (B_{10}-B_{15}-) have a triangular dense stacking planar or quasi-planar structure with a chemical bonding pattern similar to that of cyclic olefins and exhibit typical aromatic and anti-aromatic characteristics [11]. From the B_{16} to B_{20} scale range, the boron clusters begin to transition from a planar (quasi-plane) structure to a toroidal or tubular structure [16]. Later, bigger anionic boron clusters B_{16}-B_{42}- were discovered, and as their size grew, hexagonal holes started to appear in the quasi-plane structure [15, 17]. In 2014, Zhai et al., made the first cage-like all-boron fullerene cluster (boron sphere alkene) with D_{2d}-symmetry, four heptagonal holes on the waist and two staggered hexagonal holes on the top and bottom of the structure. This discovery was made using a combination of photoelectron spectroscopy and calculations from quantum chemical theory. Since then, borospherenes have garnered a great deal of interest from scientists [18].

Due to the presence of a single p-electron, the 2s and 2p electrons of boron atoms are easily hybridized to form SP^2 valence electron structures, which are very easy to bond with other atoms, especially with metals to form some cluster materials with special functions [19–21]. Li and Popov have thoroughly examined the structural and electrical characteristics of transition metal Co^- and Rh^- doped B_{12} clusters, as well as Al^- and B_9^- and B_{10}^- doped B_9^- and B_{10}^- clusters [20, 22]. Thus, metal-doped B clusters' physicochemical characteristics have drawn a lot of attention in recent years [23–25]. It demonstrates to us the significance of the doping of transition metal atoms into boron clusters in the study of metal coordination chemistry.

Alkali metal-doped boron cluster research has been described in part [23, 26]. So far, theoretical and experimental work on alkali metal-doped pure boron clusters has been widely carried out, and many characteristic research results have been obtained. Although theoretical research on potassium-doped boron clusters in alkali metals is still in its infancy, this study uses sophisticated theoretical computations to thoroughly examine the geometry, electrical characteristics, and stability of such clusters.

2 Computational details

We employed an effective optimization approach to look for the global minimum to acquire the K_2B_n cluster's ground-state structure. The CALYPSO code is the efficient method we use, which can quickly predict the most stable cluster structure using particle swarm optimization algorithms, and to narrow the search space and increase the diversity of the structures, it also inserts symmetry constraints into the structure formation process [27–29]. This method's efficacy for predicting cluster structure has been demonstrated in reference [30–39]. For K_2B_n ($n = 1$–12) structure prediction, we monitor 50 generations for each category, with each generation including 30 structures, 60% of which are produced by the pso method and the remaining 40% produced randomly. Thus, for each category, we get 1500 initial structures. At the B3LYP/6-31g level [40–43], the initial geometric optimization and energy calculations for these isomers were carried out. Subsequently, the energies are sorted from low to high and then the lower-energy structures with the top 30 are picked out for further re-optimization at various spin multiplicities. Considering the time consumption, the basis sets labeled GEN is the combination of 6-311+G(d) and def2-tzvp basis sets [44–48], which are employed for the B and K atoms, respectively. To make sure that the lowest energy structures are real minima without fictitious frequencies, the harmonic vibration frequencies are also calculated. The Gaussian 09 software program implements each of the aforementioned calculations [49, 50]. We examined the bonding characteristics of the magic clusters using the Multiwfn 3.7 program, including the Electronic Localization Function and AdNDP (Adaptive Natural Density Partitioning) [51, 52].

3 Results and discussion

3.1 Geometric structure

Figure 1 displays the K_2B_n ($n = 1$–12) clusters' ground-state configurations using the technique outlined in Sect. 2. These K_2B_n isomers should be referred to as na, nb, nc, and nd, where n is the number of B atoms, a is the ground-state structure, and b, c, and d are the metastable structures. Additionally, the relative energy (in eV) and point group symmetry are indicated beneath the structure. The ground-state cluster K_2B_n ($n = 1$–12)'s electronic states and symmetries are listed in Table 1.

The structural evolution of K_2B_n clusters ($n = 1$–12) is studied in detail, and the same K_2B_n cluster calculation method described in Sect. 2 was used to obtain the corresponding pure boron clusters as a comparison object. Compared with the earlier work [53, 54], we can see that they generally agree with our conclusions for Bn clusters, suggesting a reasonable theoretical approach to boron-based clusters. Several interesting findings came out of the structural examination of the doped clusters: (1) We discovered that the two unusual K atoms invariably take up the convex cap position in the ground-state structure of practically all K_2B_n clusters. This phenomenon might be due to the different atomic radii of the doped elements. (2) It is obvious that in the case of $n = 6$–12 and 3, the K_2B_n clusters exhibit a 3D structure, while the B_n clusters are 2D or arc structures except for the B_9 cluster which is 3D. Moreover, after K atom doping, only the conformation of $K_2B_{1,2}$ clusters retains the main skeleton of pure $B_{3,4}$ clusters. That is

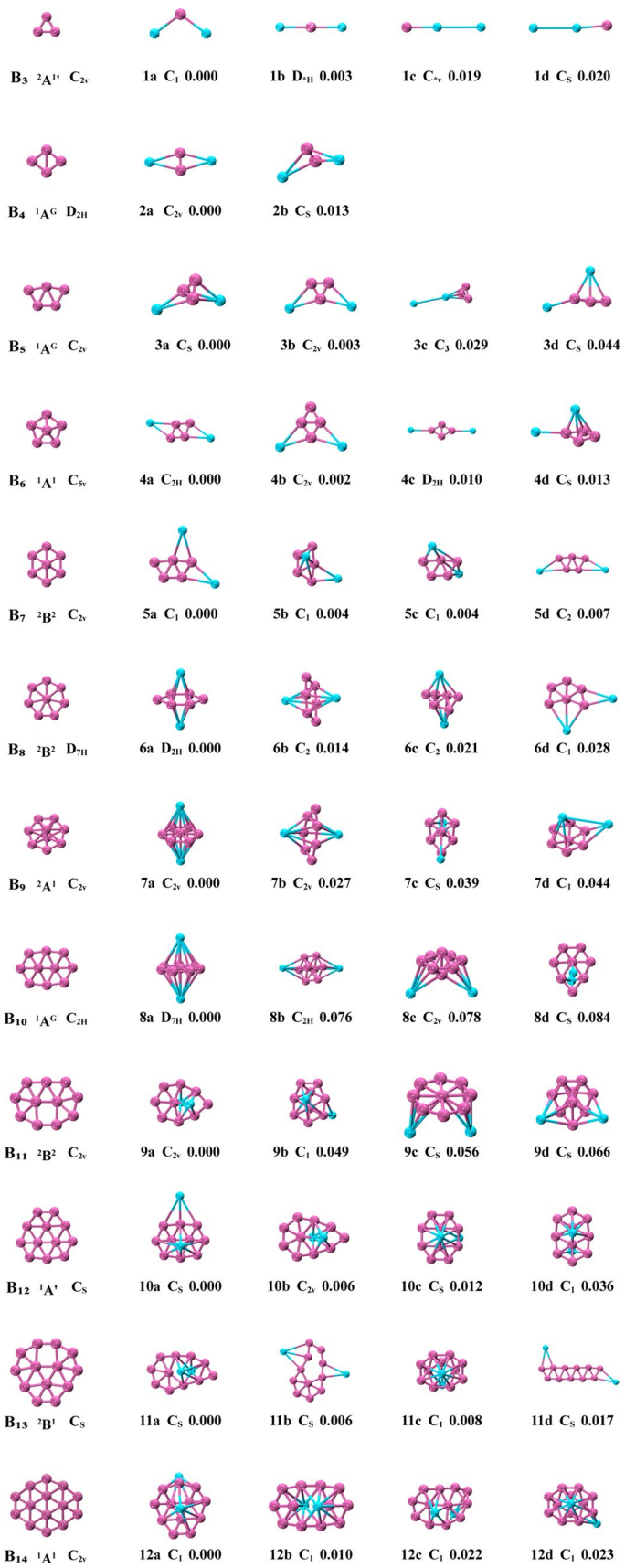

Fig. 1 Most stable structures of B_{n+2} clusters and low-lying isomers of K_2B_n ($n = 1–12$) clusters, along with the point group symmetry and relative energy (eV). The pink and blue balls represent B and K atoms, respectively

Table 1 Electronic states, symmetries, average binding energies E_b(eV), HOMO–LUMO energy gaps E_g(eV), and charges on the K atoms of the most stable K_2B_n(n = 1–12) clusters

Clusters	K_2B_n					
					Charge	
	sta	sym	E_b	E_g	K-1	K-2
$n=1$	^{4}A"	C_s	0.54	1.33	0.582	0.582
$n=2$	$^3A_1$	C_{2v}	1.66	1.82	0.791	0.791
$n=3$	^{2}A"	C_s	2.44	1.59	0.829	0.826
$n=4$	$^2A_1$	C_{2h}	2.83	1.65	0.866	0.866
$n=5$	^{2}A	C_1	3.17	1.62	0.874	0.898
$n=6$	^{1}A'	D_{2h}	3.48	2.81	0.926	0.926
$n=7$	$^2B_1$	C_{2v}	3.72	1.49	0.933	0.924
$n=8$	$^1A_1$	D_{7h}	4.07	3.31	0.930	0.930
$n=9$	$^2A_1$	C_{2v}	4.06	2.66	0.931	0.931
$n=10$	1A'	C_s	4.16	2.11	0.948	0.845
$n=11$	^{2}A"	C_s	4.15	1.47	0.930	0.929
$n=12$	^{1}A	C_1	4.29	2.11	0.838	0.936

to say, the two doped K atoms result in a clear structural reconfiguration phenomenon for the K_2B_n ($n=3$–12) cluster ground-state structure. (3) K_2B_n clusters expand by covering the surface of K_2B_{n-1} clusters with boron atoms when the number of B atoms increases between $n=1$–3 and $n=6$–12. K_2B_5 is also grown with a boron atom overlaid on K_2B_4, with the difference that the orientation of the two K atoms has changed.

3.2 Relative stability and charge transfer

The average binding energy (E_b) and second-order difference of energy (Δ^2E) can be used to describe the cluster's stability, where the E_b indicates how much the average energy per atom increases after breaking the cluster into single atoms. The clusters are defined as follows, and the more stable they are, the greater the values of E_b and Δ^2E.

$$E_bK_2B_n = \frac{nE(B) + 2E(K) - E\left[K_2B_n\right]}{n+2} \quad (1)$$

$$\Delta^2E\left(K_2B_n\right) = E\left(K_2B_{n+1}\right) + E\left(K_2B_{n-1}\right) - 2E\left(K_2B_n\right) \quad (2)$$

where the energy E in the equation corresponds to the energy of an individual atom or atom cluster. The results of the calculations based on the above equation are plotted in Fig. 2. As shown in (A), the E_b value of the K_2B_n cluster increases sharply with the increase of B atoms at $n=1$–8 and is in an oscillating trend at $n=8$–12. However, the E_b growth rate of the B cluster is significantly lower than that of the K_2B_n cluster, so the E_b values of both are approaching $n=1$–8. It is easy to find a clear local maximum peak for the K_2B_n cluster at $n=8$, indicating that it is more stable than the surrounding structures. In addition, most of the identification evidence for stable clusters may be inferred by the maximum value of Δ^2E compared to its neighbors. In (B), several different peaks can be found, K_2B_3, K_2B_6, K_2B_8, and K_2B_{10}, especially the K_2B_8 cluster has the largest Δ^2E value of 3.29 eV. These peaks imply extraordinary stability for these isomers.

Next, we looked at how the distance E_g (HOMO–LUMO gap) between a cluster's highest occupied (HOMO) and lowest unoccupied (LUMO) molecular orbitals changes as cluster size rises. We calculated the gap E_g for K_2B_n ($n=1$–12) and B_n ($n=3$–15) and plotted it in (C). For the K_2B_n clusters, the HOMO–LUMO gap shows irregular parity oscillation behavior with several distinct maxima at $n=2$, 4, 6, and 8, indicating their higher chemical stability [55–59]. In the range of $n=1$–5, 8–9, and 10–12, pure B clusters and K_2B_n clusters have the same trend, but because of the addition of doped atoms at $n=6$ and 7, both show reverse oscillation compared to E_g values. In addition, the curves about the pure boron clusters in Fig. 2 are all consistent with the previous studies.

3.3 Charge transfer

The charge (Q) distribution of K atoms in the K_2B_n ($n=1$–12) cluster is listed in Table 1, which we obtained using the natural population analysis (NPA). The results show that among all the K_2B_n ($n=1$–12) clusters, the K atom is positively charged because it acts as an electron donor. In other words, the charge is transferred from the K atom to the B backbone of all neutral substances. This might be a result of the lesser Pauline electronegativity of the K atom (0.82) compared to the B atom (2.04). By observing the charge relations of (Table 1) K atoms, we found that at $n=1$–6, the positive charge on the K atom rises quickly, climbs gradually at $n=6$–9, reaches a maximum at $n=9$, and then begins to

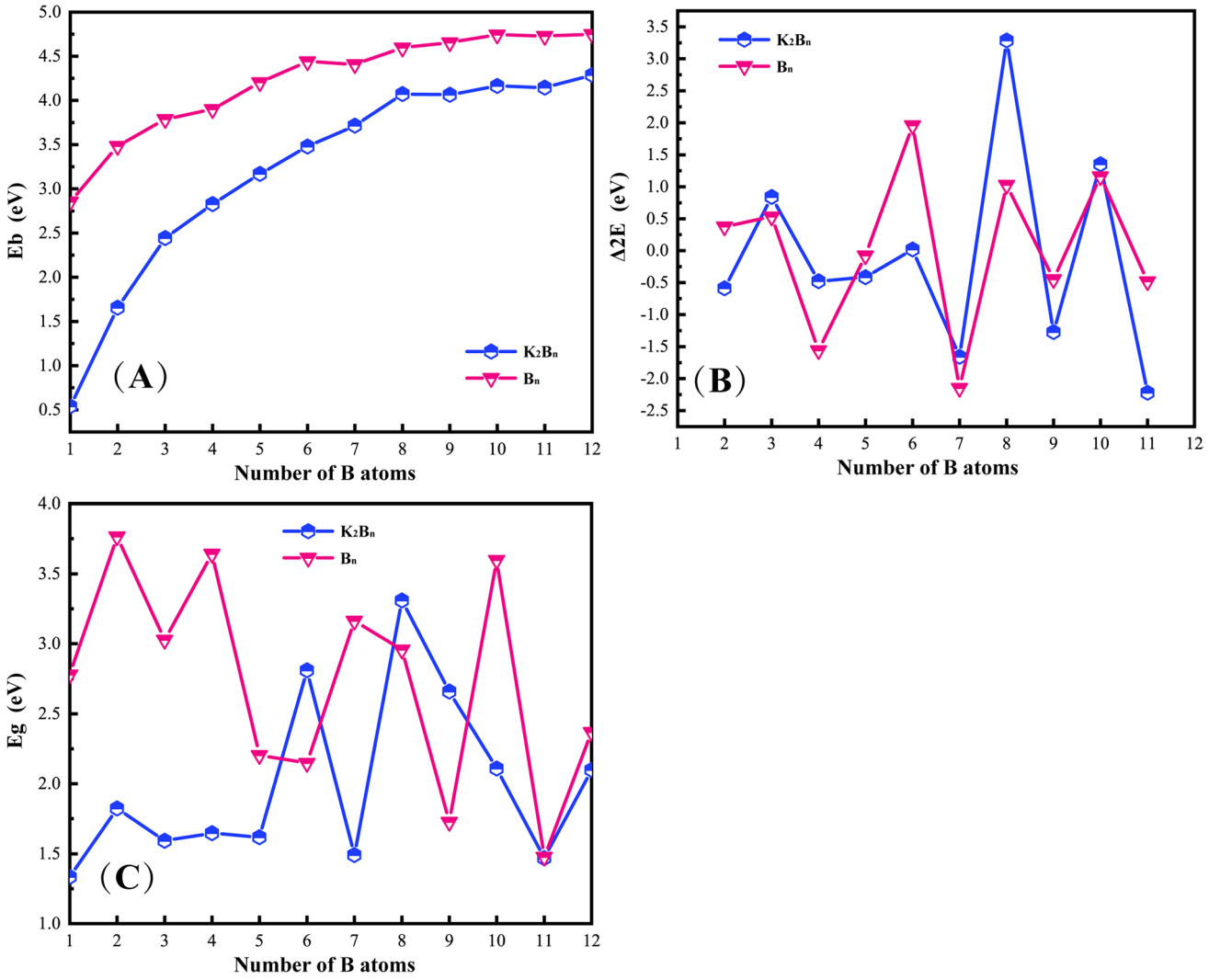

Fig. 2 Size dependence of the average binding energy E_b (**A**), the second-order difference of energy $\Delta_2 E$ (**B**), HOMO–LUMO energy gaps E_g (**C**)

oscillate. The charge transfer of each ground-state structure in the K_2B_n system exceeds 1e. This implies that the neutral potassium-doped boron clusters are more likely to generate stronger K–B bonds. Not to be disregarded is the fact that K2B8's charge transfer reaches 1.86e, which may contribute to its notable stability.

3.4 Bonding characters

From the above analysis, the E_b, $\Delta^2 E$, $E_{g,}$ and charge transfer were considered together and K_2B_8 was found to exhibit good stability. We further analyzed the characteristics of molecular orbitals (Mos) and the bonding characteristics of this cluster to delve deeper into the deeper causes of its exceptional stability. First, we looked at the cluster's DOS (density of state), as seen in Fig. 3, to qualitatively assess the contribution of the doped K atom and B skeletons to the low-energy MO chemical bond. We note that when the orbital energy is between − 21.77 eV and − 18.5 eV, the total density of state (TDOS) is almost from the contribution of doped atom K. The contribution of B atoms accounts for the full TDOS when the orbital energy is between − 16.33 eV and − 2.72 eV. When the orbital energy is higher than 0 eV, the contribution of B atoms to the TDOS in the structure is significantly larger than that of K atoms. Second, portions of the K_2B_8 cluster's molecular orbital diagrams, together with the accompanying energy levels and HOMO–LUMO energy gaps, were created to better comprehend the molecular orbitals of the cluster (see Fig. 4). According to the findings, K_2B_8 had a HOMO energy of − 4.47 eV and a LUMO value that was 3.31 eV greater. In detail, the component of HOMO is mainly from 96.91% of p atom orbitals (AO) of B atoms in the main framework; the component of LUMO is mainly from 69.67% of s AO and 21.18% of p AO of two doped K

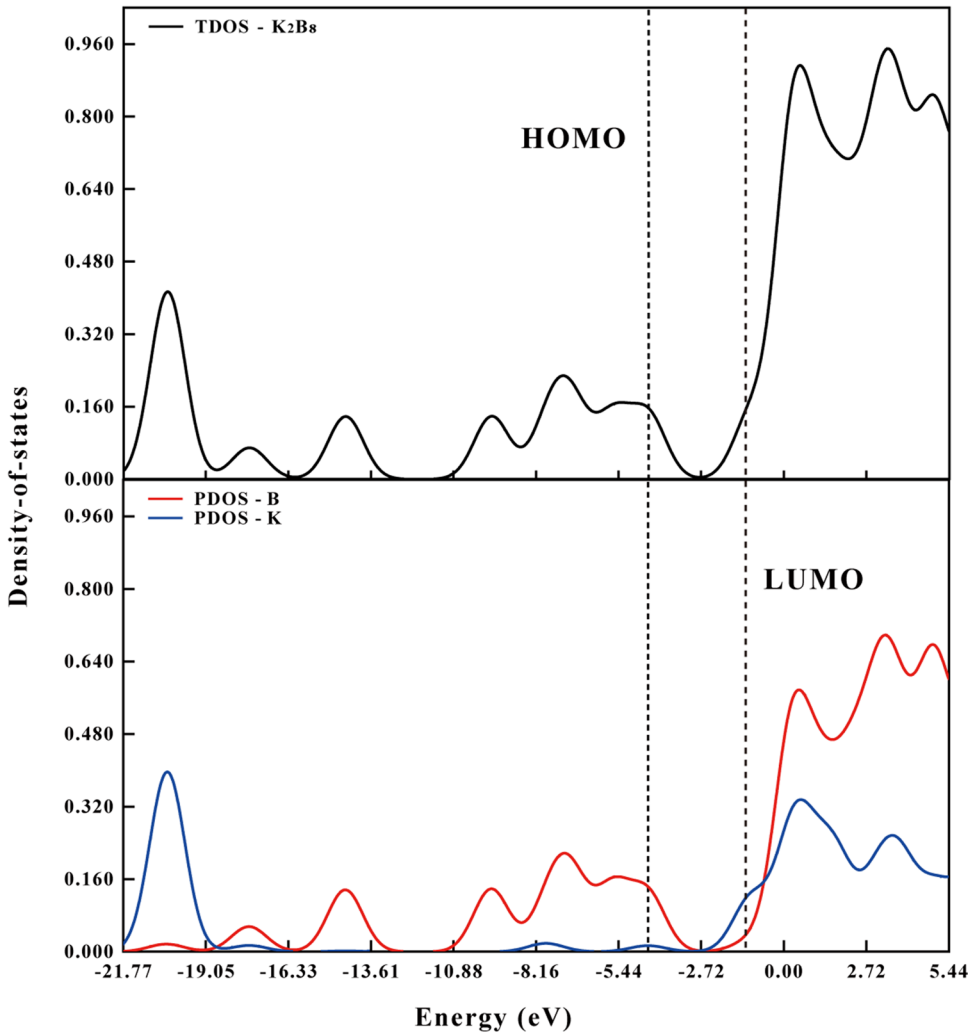

Fig. 3 Calculated TDOS (total densities of states) and PDOS (partial densities of states) of the K_2B_8 cluster

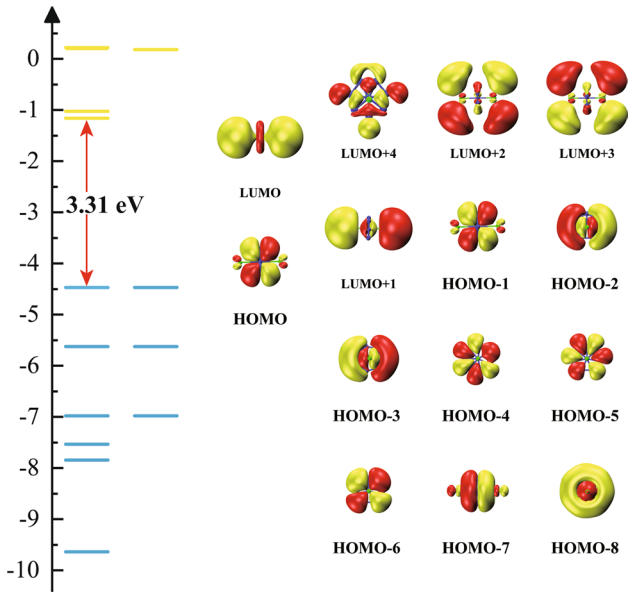

Fig. 4 Molecular orbitals and the corresponding energy levels of the K_2B_8 cluster. The HOMO–LUMO gap is indicated (in red)

atoms. The contributions of the p AO of the K atom, the s and p AO of the B atoms, and the HOMO-2 and HOMO-3 occupied molecular orbitals are 1.15%, 21.49%, and 73.02%, respectively, for the other occupied molecular orbitals. K atoms' and B atoms' respective s and p AO to HOMO-7 are 0.61%, 1.03%, 0.61%, and 96.98%. These analytical results imply that the main constituents of these molecular orbitals are K-p AOs, B-s AOs, and B-p AOs. In other words, the K-B and B-B s-p hybridization encourages the engagement of the doped K atom with the B_8 fragment and the notable stability of the K_2B_8 cluster.

It is well known that examining the bonding properties of K_2B_8 requires an understanding of the composition of its multicenter bonds. Specifically, we applied the adaptive natural density partitioning (AdNDP) approach to a systematic search for N-centered two-electron (nc–2e) bonds. The primary criterion is that a bond is deemed to have a localized character when $n \leq 2$, and a delocalized character otherwise. The schematic structure of the K_2B_8 cluster, the occupation numbers (ONs) of the multicenter bonds, and the structural

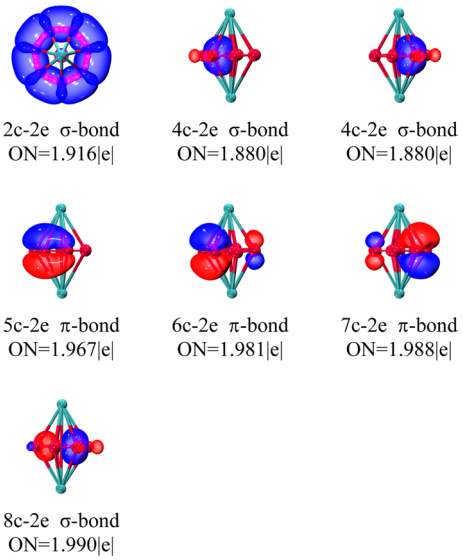

Fig. 5 AdNDP chemical bonds for the K_2B_8 cluster. ON denotes the occupation number

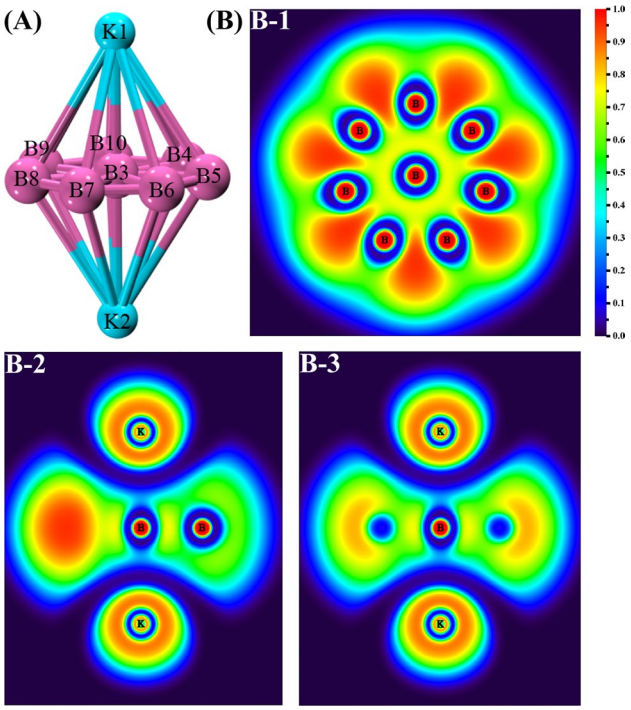

Fig. 6 Analysis of ELF **A** the structural diagram with all atomic labels, **B** 2D color distribution of the ELF projection in different planes of the K_2B_8 cluster

units corresponding to the multicenter bonds are shown in Fig. 5. The analyzed structure after systematic search shows that there are no definite domain bonds in K_2B_8, but there are 13 delocalized bonds. Among them, the atoms flanking the double pagoda-like structure form ten σ-type bonds, namely seven 2c–2e bonds (occupation number ON = 1.916|e|), two 4c–2e bonds (occupation number ON = 1.88|e|), and one 8c–2e bond (occupation number ON = 1.99|e|). The remaining 5c–2e, 6c–2e, and 7c–2e (whose occupation numbers are ON = 1.967|e|, 1.981|e| and 1.988|e|, respectively) exhibit π-type features. Overall, it is clear that the doped K atoms have a higher likelihood of forming N-centered two-electron (nc–2e) bonds with larger occupation numbers together with their nearby B atoms.

However, to learn more about the bond properties of the K_2B_8 cluster, the electron localization function (ELF) was examined. The results are presented in Fig. 6. The three-dimensional real space function ELF has values between 0 and 1. In essence, the region with the higher value of the ELF is surrounded by an analogous surface where the electrons are more locked and less likely to escape, allowing them to travel more freely in comparison (in this region at will out of the domain). The electron localization is weak in certain places with low ELF values; therefore, if the electrons are positioned there, they can readily leave the domain and move to other parts. As seen in Fig. 6, some places between the K2B8 (B–B, K–B, K–K) atoms are visible as yellow–green or even orange in the ELF projections in different planes, indicating that the ELF values in these regions are more than 0.5, indicating that covalent bonds are formed in the B–B, K–B, and K–K connecting regions. It is intriguing that these higher electron localization joining locations are uniformly skewed in favor of the B atom, which is consistent with the findings of earlier charge transfers.

4 Conclusion

In conclusion, the DFT calculations at the B3LYP energy level and the CALYPSO structure search method were used to conduct a systematic investigation of the potassium-doped boron clusters. The ground-state structures of clusters of different sizes were identified based on their total energy and point group symmetry after a significant number of stable low-energy structures were obtained. The impurity K atom likes the convex top position of the backbone in all of the most stable K_2B_n structures. The doped K atom consistently serves as an electron donor in the K_2B_n ($n = 1–12$) cluster range. The K_2B_8 clusters with a double pagoda structure showed good stability in this study, according to the analysis of the clusters' relative stability and charge transfer. The work specifically shows that the s-p hybridization of B–B and B–K made a substantial contribution to the good stability of the K_2B_8 clusters by further analyzing the molecular orbitals and chemical bonds of K_2B_8. Our study is intended to serve as a guide for the future synthesis and use of doped boron-based nanomaterials.

Acknowledgements The authors are grateful to the Innovation Fund of Postgraduate Sichuan University of Science & Engineering (Grant No. y2021008, Y2022013, Y2022014), the Cultivating Program of Young and Middle-aged Backbone Teachers of Chengdu University of Technology (No. 10912-JXGG2022-09146), and the Innovation and Entrepreneurship Training Program of Sichuan Province (Grant No. S202110622032). This work was supported by Sichuan University of Science & Engineering High Performance Computing Center provided computational.

References

1. H.-G. Jang et al., Synthesis of dimesitylborane-substituted phenylcarbazoles as bipolar host materials and the variation of the green PHOLED performance with the substituent position of the boron atom. Dalton Trans. **43**(21), 7712–7715 (2014)
2. M.-S. Lin et al., A diarylborane-substituted carbazole as a universal bipolar host material for highly efficient electrophosphorescence devices. J. Mater. Chem. **22**(3), 870–876 (2012)
3. M.-M. Xue et al., De novo design of boron-based host materials for highly efficient blue and white phosphorescent OLEDs with low efficiency roll-off. ACS Appl. Mater. Interfaces. **8**(31), 20230–20236 (2016)
4. J.-I. Aihara, B13+ is highly aromatic. J. Phys. Chem. A **105**(22), 5486–5489 (2001)
5. I. Boustani, Systematic lsd investigation on cationic boron clusters: B (n 2–14). Int. J. Quant. Chem. **52**(4), 1081–1111 (1994)
6. L. Hanley, J.L. Whitten, S.L. Anderson, Collision-induced dissociation and ab initio studies of boron cluster ions: determination of structures and stabilities. J. Phys. Chem. **92**(20), 5803–5812 (1988)
7. H.J. Zhai et al., Hepta-and octacoordinate boron in molecular wheels of eight-and nine-atom boron clusters: observation and confirmation. Angew. Chem. Int. Ed. **42**(48), 6004–6008 (2003)
8. B. Albert, H. Hillebrecht, Boron: elementary challenge for experimenters and theoreticians. Angew. Chem. Int. Ed. Engl. **48**(46), 8640–8668 (2009)
9. J.-I. Aihara, H. Kanno, T. Ishida, Aromaticity of planar boron clusters confirmed. J. Am. Chem. Soc. **127**(38), 13324–13330 (2005)
10. A.N. Alexandrova et al., Electronic structure, isomerism, and chemical bonding in B7-and B7. J. Phys. Chem. A **108**(16), 3509–3517 (2004)
11. A.N. Alexandrova et al., All-boron aromatic clusters as potential new inorganic ligands and building blocks in chemistry. Coord. Chem. Rev. **250**(21–22), 2811–2866 (2006)
12. K.C. Lau, R. Pandeyl, The 2D–3D structural transition and chemical bonding in. Struct. Propert. Clusters Few Atoms Nanoparticles **5**, 116 (2006)
13. H.-J. Zhai et al., Hydrocarbon analogues of boron clusters—planarity, aromaticity and antiaromaticity. Nat. Mater. **2**(12), 827–833 (2003)
14. A.P. Sergeeva et al., All-boron analogues of aromatic hydrocarbons: B17− and B18−. J. Chem. Phys. **134**(22), 224304 (2011)
15. A.P. Sergeeva et al., Understanding boron through size-selected clusters: structure, chemical bonding, and fluxionality. Acc. Chem. Res. **47**(4), 1349–1358 (2014)
16. M.P. Johansson, On the strong ring currents in B20 and neighboring boron toroids. J. Phys. Chem. C **113**(2), 524–530 (2009)
17. L.-S. Wang, Photoelectron spectroscopy of size-selected boron clusters: from planar structures to borophenes and borospherenes. Int. Rev. Phys. Chem. **35**(1), 69–142 (2016)
18. H.-J. Zhai et al., Observation of an all-boron fullerene. Nat. Chem. **6**(8), 727–731 (2014)
19. T.R. Galeev et al., Observation of the highest coordination number in planar species: decacoordinated Ta© B10− and Nb© B10− anions. Angew. Chem. Int. Ed. **51**(9), 2101–2105 (2012)
20. W.-L. Li et al., Aluminum avoids the central position in AlB9–and AlB10–: photoelectron spectroscopy and ab Initio study. J. Phys. Chem. A **115**(38), 10391–10397 (2011)
21. C. Romanescu et al., Aromatic metal-centered monocyclic boron rings: Co© B8− and Ru© B9−. Angew. Chem. **123**(40), 9506–9509 (2011)
22. I.A. Popov et al., Complexes between planar boron clusters and transition metals: a photoelectron spectroscopy and ab initio study of CoB12–and RhB12–. J. Phys. Chem. A **118**(37), 8098–8105 (2014)
23. A.N. Alexandrova et al., Molecular wheel B82-as a new inorganic ligand. Photoelectron spectroscopy and ab initio characterization of LiB8. Inorgan. Chem. **43**(12), 3552–3554 (2004)
24. J.-B. Gu et al., Structural, electronic, and magnetic properties of boron cluster anions doped with aluminum: BnAl−(2≤ n≤ 9). Chin. Phys. B **21**(4), 043102 (2012)
25. Z.-F. Liu et al., A density-functional theory for (BAs) n clusters (n= 1–14): structures, stabilities and electronic properties. Chin. Phys. B **20**(2), 023101 (2011)
26. H.-J. Zhai et al., Electronic structure and chemical bonding of B 5− and B 5 by photoelectron spectroscopy and ab initio calculations. J. Chem. Phys. **117**(17), 7917–7924 (2002)
27. J. Lv et al., Particle-swarm structure prediction on clusters. J. Chem. Phys. **137**(8), 084104 (2012)
28. Y. Wang et al., Crystal structure prediction via particle-swarm optimization. Phys. Rev. B **82**(9), 094116 (2010)
29. Y. Wang et al., CALYPSO: a method for crystal structure prediction. Comput. Phys. Commun. **183**(10), 2063–2070 (2012)
30. D. Die et al., The ground-state structure, optical-absorption and photoelectron spectrum of silver clusters. Phys. E **117**, 113805 (2020)
31. L.-P. Ding et al., Structures, mobilities, and electronic properties of functionalized silicene: Superhalogen BO2 adsorption. Inorg. Chem. **59**(7), 5041–5049 (2020)
32. Y.-W. Fan, H.-Q. Wang, H.-F. Li, Structural and electronic properties of exohedrally doped neutral silicon clusters LnSi n (n= 5, 10; Ln= Sm, Eu, Yb). Phys. Chem. Chem. Phys. **22**(36), 20545–20552 (2020)
33. L. Lai et al., Growth mechanism and electronic and magnetic properties of AgnTi alloy clusters. J. Phys. Chem. Solids **148**, 109757 (2021)
34. C.-G. Li et al., Analysis of the structures, stabilities and electronic properties of MB 16−(M= V, Cr, Mn, Fe Co, Ni) clusters and assemblies. New J. Chem. **44**(13), 5109–5119 (2020)
35. C.-G. Li et al., A comparative study of Cu n X (X= Sc, Y; n= 1–10) clusters based on the structures, and electronic and aromatic properties. New J. Chem. **43**(17), 6597–6606 (2019)
36. Z. Li et al., The selectivity of the transition metal encapsulated in fullerene-like B36 clusters. Chem. Phys. Lett. **757**, 137876 (2020)
37. C. Lu, C. Chen, Indentation strengths of zirconium diboride: intrinsic versus extrinsic mechanisms. J. Phys. Chem. Lett. **12**(11), 2848–2853 (2021)
38. C. Lu et al., Elucidating stress–strain relations of ZrB12 from first-principles studies. J. Phys. Chem. Lett. **11**(21), 9165–9170 (2020)
39. Y.R. Zhao et al., Probing the structural and electronic properties of neutral and anionic lanthanum-doped silicon clusters. J. Phys. Chem. C **123**(47), 28561–28568 (2019)
40. S.M. Bouzzine et al., Density functional theory (B3LYP/6-31G*) study of oligothiophenes in their aromatic and polaronic states. J. Mol. Struct. (Thoechem.) **726**(1–3), 271–276 (2005)
41. J.E. Del Bene, W.B. Person, K. Szczepaniak, Properties of hydrogen-bonded complexes obtained from the B3LYP functional with

6–31G (d, p) and 6–31+ G (d, p) basis sets: comparison with MP2/6-31+ G (d, p) results and experimental data. J. Phys. Chem. **99**(27), 10705–10707 (1995)
42. H. Kruse, L. Goerigk, S. Grimme, Why the standard B3LYP/6-31G* model chemistry should not be used in DFT calculations of molecular thermochemistry: understanding and correcting the problem. J. Org. Chem. **77**(23), 10824–10834 (2012)
43. J. Tirado-Rives, W.L. Jorgensen, Performance of B3LYP density functional methods for a large set of organic molecules. J. Chem. Theory Comput. **4**(2), 297–306 (2008)
44. T.M. Krygowski, J.E. Zachara, H. Szatylowicz, Molecular geometry as a source of chemical information. 3. How H-bonding affects aromaticity of the ring in the case of phenol and p-nitrophenol complexes: A B3LYP/6–311+ G** study. J. Org. Chem. **69**(21), 7038–7043 (2004)
45. X. Li et al., Pentaatomic tetracoordinate planar carbon,[CAl4] 2−: a new structural unit and its salt complexes. Angew. Chem. **112**(20), 3776–3778 (2000)
46. Z. Liu, T. Lu, Q. Chen, An sp-hybridized all-carboatomic ring, cyclo [18] carbon: Electronic structure, electronic spectrum, and optical nonlinearity. Carbon **165**, 461–467 (2020)
47. F. Weigend, Accurate Coulomb-fitting basis sets for H to Rn. Phys. Chem. Chem. Phys. **8**(9), 1057–1065 (2006)
48. F. Weigend, R. Ahlrichs, Balanced basis sets of split valence, triple zeta valence and quadruple zeta valence quality for H to Rn: Design and assessment of accuracy. Phys. Chem. Chem. Phys. **7**(18), 3297–3305 (2005)
49. M. Frisch et al., in *Gaussian 09, revision D. 01*. 2009, Gaussian, Inc., Wallingford CT (2009)
50. M.E. Frisch et al., in *Gaussian, Inc., Wallingford CT*. Wallingford CT (2009).
51. T. Lu, F.-W. Chen, Meaning and functional form of the electron localization function. Acta Phys. Chim. Sin. **27**(12), 2786–2792 (2011)
52. D.Y. Zubarev, A.I. Boldyrev, Developing paradigms of chemical bonding: adaptive natural density partitioning. Phys. Chem. Chem. Phys. **10**(34), 5207–5217 (2008)
53. L. Cheng, B14: an all-boron fullerene. J. Chem. Phys. **136**(10), 104301 (2012)
54. R. Kawai, J. Weare, Instability of the B12 icosahedral cluster: rearrangement to a lower energy structure. J. Chem. Phys. **95**(2), 1151–1159 (1991)
55. A. Jalbout, S. Fernandez, Part II. Gaussian, complete basis set and density functional theory stability evaluation of the singlet states of Cn (n= 1–6): energy differences, HOMO–LUMO band gaps, and aromaticity. J. Mol. Struct. Theochem. **584**(1–3), 169–182 (2002)
56. J.-I. Aihara, Weighted HOMO-LUMO energy separation as an index of kinetic stability for fullerenes. Theoret. Chem. Acc. **102**, 134–138 (1999)
57. R. Rakhi, C.H. Suresh, A DFT study on dihydropyrazine annulated linear polyacenes: aromaticity, stability and HOMO–LUMO energy modulation. Phys. Chem. Chem. Phys. **18**(35), 24631–24641 (2016)
58. S. Neukermans et al., Extremely stable metal-encapsulated AlPb 10+ and AlPb 12+ clusters: mass-spectrometric discovery and density functional theory study. Phys. Rev. Lett. **92**(16), 163401 (2004)
59. S. Burkart et al., Experimental verification of the high stability of Al13H: a building block of a new type of cluster material? Chem. Phys. Lett. **301**(5–6), 546–550 (1999)